# Chemical functionalization of the graphene surface for electrical and electrochemical sensing applications

Jiang, L.

# Chapter 1

## Introduction

Part of this chapter was published as a review article: Wangyang Fu, Lin Jiang, Erik P. van Geest, Lia M. C. Lima, and Grégory F. Schneider, *Adv. Mater.* **2017**, 29, 1603610.

Graphene is a two-dimensional (2D) carbon allotrope composed of a single layer of $sp^2$ hybridized atoms arranged in a hexagonal lattice. Figure 1.1a shows the honeycomb lattice of graphene containing atom A and atom B in each unit cell. As the $sp^2$ orbitals contribute to form the plane, the unsaturated perpendicular $p_z$ orbitals form an extended π-band with delocalized electrons. The conduction π* band and valence π band meets each other at the so-called Dirac point (*K* and *K'*) or charge neutrality point, forming a zero bandgap semiconductor (Figure 1.1b). At the low energies that are most relevant in electron transport, the electrons behave in a linear dispersion with the band structure viewed as two conical cones (Dirac cones, Figure 1.1c). As illustrated in Figure 1d, the density of states (DOS) varies linearly with the energy in each Dirac cone. More importantly, such an unique band structure contribute to the intrinsic charge carrier mobility of graphene at room temperature, which can be as high as 15000 $cm^2\ V^{-1}\ s^{-1}$.[1]

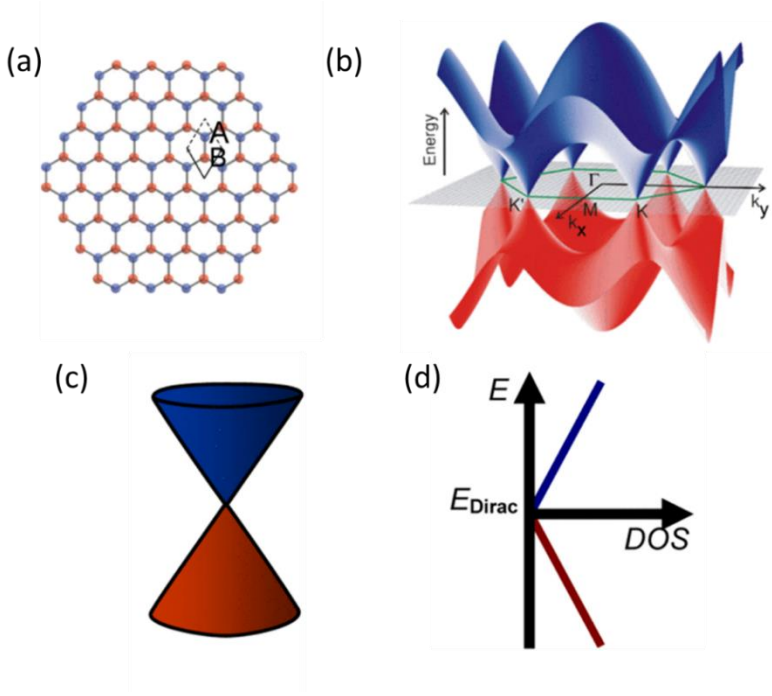


**Figure 1.1 Graphene lattice and band structure.** a) The honeycomb lattice. b) The electronic band structure. b) Linear dispersion at low energies. c) Density of states (DOS) dependence on energy.[2]

In addition to the extraordinarily high mobility, graphene is also characterized with a low intrinsic electrical noise[3] and inert chemical properties. All these properties render the graphene basal plane an ideal candidate for electrical and electrochemical studies. In particular, nanoelectronics based on the surface of graphene provide a

versatile platform for a wide spectrum of (bio)chemical sensing applications.[4] Detection can be realized through various mechanisms, including charge transfer,[5] charge scattering,[6] capacitive effect,[7] and field effect[8]. In particular, the electrical field effect has been widely regarded as one of the most reliable sensing mechanisms.

## 1.1 Graphene field-effect transistors (GFETs)

Since the experimental preparation and observation of the electric field effect in graphene by the Manchester group in 2004,[9] biochemical sensing using graphene electronic devices has been actively pursued.[10] The sensing principle rests on a change of the electrical conductance of the graphene channel upon adsorption of a molecule on the sensor surface.[10a] The uniqueness of graphene among other solid-state materials is that all carbon atoms are located on the surface, making the graphene surface potentially highly sensitive to any changes of its surrounding environment. For instance, the chemisorption of gas molecules on the graphene surface has been reported with the sensitivity down to a single molecule detection,[10a] which is mainly ascribed to the surface contaminations by polymer residues during device fabrication.[11]

### *1.1.1 Back-gated GFETs*

The word transistor is a combination of two words: transfer and resistor. Usually a transistor is used to switch or amplify an electronic signal, comparable to a tap-valve that controls the supply and flow of water. Figure 1.2a depicts a back-gated GFET composed of a source/drain metallic electrode bridged together with a graphene channel. The carrier density, and thus the conductivity of the channel is typically modulated by the electric field via gating a highly conductive silicon substrate located underneath an insulating $SiO_2$ dielectric layer to a range of voltages. As shown in Figure 1.2b, a typical measurement consists in applying a constant bias voltage, $V_{sd}$, between the source and the drain of the graphene channel, and monitoring the resulting source-drain current $I_{sd}$. By changing the back gate voltage $V_g$, the electrochemical potential of the charge carriers (i.e., the Fermi energy) can be modulated. As a consequence, the type of charge carriers (which flow in the graphene channel and give the current $I_{sd}$) can continuously be tuned from holes (red curve in the left of Figure 1.2b) to electrons (grey curve in the right of Figure 1.2b), yielding a so-called 'ambipolar behavior'. At the transition between the electron and hole regime, the current (conductivity) is minimized and this point is also known as the charge neutrality point (CNP).

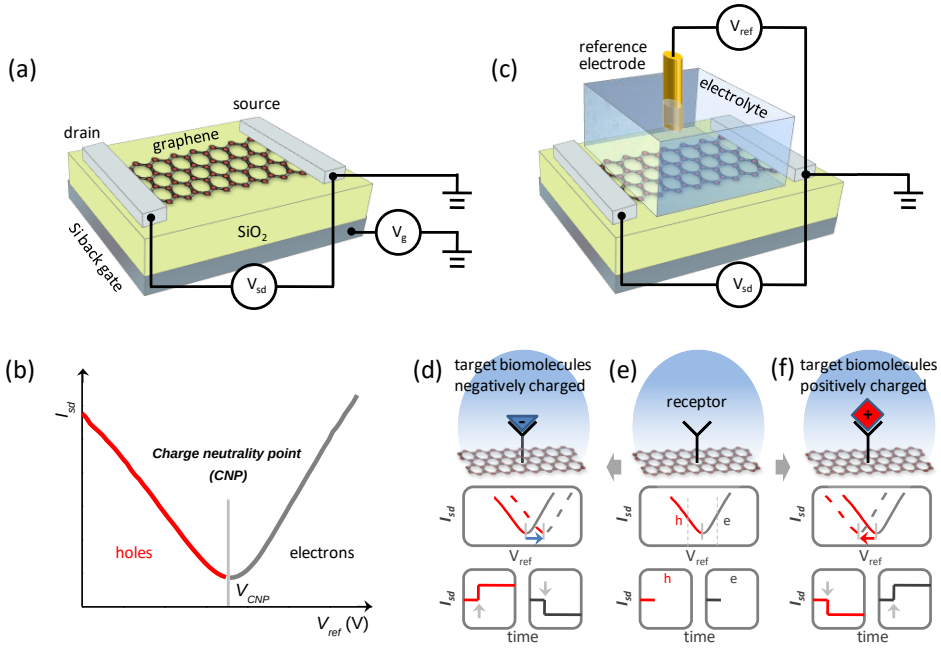


**Figure 1.2 Working principle of a graphene field-effect transistor (GFET).** a) Schematic of a back-gated GFET. b) Typical ambipolar transfer characteristics showing that the type of carriers in graphene can continuously be modulated from holes (on the left, in red) to electrons (on the right, in grey) using the field effect. The charge-neutrality point (CNP) is located at the transition between the electron and hole regime, where the current is minimized. c) Schematic of an electrochemically-gated GFET device and its sensing principle (d-f). In the upper panel of e), a receptor molecule is immobilized on the graphene surface. The plots of $I_{sd}$ versus $V_{ref}$ and $I_{sd}$ versus the time $t$ are shown in the middle and lower panels, respectively. The abbreviation 'h' in red refers a measurement carried in the hole regime (and 'e' for the electron regime in grey). f) (respectively d) depicts the field effect resulting from the binding of a positively (respectively negatively) charged target on the receptor (as indicated by the grey arrows in the $I_{sd}(t)$ curves). The binding of a charged target as indicated by the blue arrows yields a shift in the curves of $I_{sd}$ versus $V_{ref}$.

### *1.1.2 Electrochemically-gated GFETs*

A change in the electric field can either be achieved using the above discussed back-gate voltage or be induced by physisorption or chemisorption of the target molecules. When the back-gate is held at a fixed voltage the change in current between the drain and source must thus be due to molecules adsorbed on the graphene surface, as demonstrated in a pioneering study by the Manchester group in 2007 with single molecule detection capability upon $NO_2$ chemisorption.[10a]

In contrast to the back-gate geometry, in an electrochemically-gated configuration the

gate voltage is applied to the electrolyte via a reference electrode (Figure 1.2c). The reference electrode is coupled to the graphene channel through an interfacial capacitance $C$, consisting of a series of two capacitances,[12] namely the quantum capacitance of graphene ($C_Q$),[13] and the double layer capacitance of the electrolyte ($C_{DL}$).[14] The double layer capacitor is a virtual capacitor formed by the separated charges located at the solid side and the solution side of the interface as described by the Poisson-Boltzmann equation.[15] Electrochemically-gated GFETs belong to the large family of ion-sensitive FETs, the first new concept of which was investigated by Bergveld with Si devices.[16] Although the choice of the channel materials, the reference electrode, the operational mode, and the final encapsulation for liquid handling, vary from case to case, the heart of any ion-sensitive FETs lies on the interface between electrolyte and the solid FET materials. In general, GFETs are operated at low electrolyte gate voltage such that any electrochemical processes and exchange ionic currents are negligible, i.e., the interface is considered to be inert and purely capacitive, although this assumption is not always explicitly stated in most of the literature. Experimental artifacts at moderate or relatively high electrolyte gate voltages resulting from such simple assumption are considered mainly of electrochemical nature.

The working principle of an electrochemically-gated GFET sensor is illustrated in Figure 1.2d-f. In practice, electrochemically-gated GFETs can be integrated into microfluidic systems:[17] the confinement into the fluidic channel helps in bringing the analyte to the sensor surface.[18] In a typical measurement, receptor molecules are immobilized on the surface for selective recognition of target molecules (Figure 1.2e, upper panel). The corresponding $I_{sd}$ versus $V_{ref}$ curve of such an electrochemically-gated GFET is shown in the middle panel (Figure 1.2e) with similar characteristics as the one observed for a back-gated GFET (Figure 1.2b). The lower panel of Figure 1.2e depicts the time dependent current $I_{sd}$ at a fixed reference potential $V_{ref}$ (as indicated by the dashed grey lines). In either the hole regime (as indicated by 'h') or in the electron regime ('e'), when a positively charged target binds (Figure 1.2f, upper panel), a depletion of hole carriers (respectively an accumulation of electron carriers) in the graphene occurs due to the field effect. Such doping effect causes a negative shift of the $I_{sd}(V_{ref})$ curve as indicated by the blue arrow in Figure 1.2f (middle panel). In the time-dependent measurement (i.e., the lower panel of Figure 1.2f), the binding of a positively charged target causes a decrease of the current $I_{sd}$ in the hole regime, and an increase of the current in the electron regime. Conversely, the binding of a negatively charged target (Figure 1.2e) induces a positive shift of the $I_{sd}(V_{ref})$ curve and an increase in the $I_{sd}$ in the hole regime. In the electron regime – instead – the same event induces a negative shift of the $I_{sd}(V_{ref})$ curve and a decrease of the current

$I_{sd}$. This current modulation in the graphene channel can be expressed as a function of the change in the carrier density $\Delta n$, which is induced by and is proportional to the total number $N$ of charged molecules adsorbing on the graphene surface:[19]

$$\Delta I_{sd} = \frac{w}{l} V_{sd} e\mu \Delta n \propto N \qquad (1)$$

where $w$ and $l$ are the width and length of the graphene channel, $e$ is the electron charge, and $\mu$ is the charge carrier mobility. In Equation (1), it is clear that the sensing response of a transistor sensor should be proportional to the total number of adsorbed molecules $N$. The quantitative monitoring of molecules, however, is non-trivial. Challenges lie in characterizing the number of charges each molecule carry, in controlling the chemical functionalization, and in identifying the exact sensing reactions at the graphene surface in each different regime. It is of note here that, in principle, non-charged molecules should have no influences on the field-effect sensing response of GFET sensors, unless they can induce a charge variation (for example, through subtle dipole fluctuation[20] or molecular engineering[21]). To deduce Equation (1), it is assumed that graphene has a constant carrier mobility $\mu$ upon the adsorption of charged molecules. This assumption is correct in most cases where the adsorbed molecules bind to the receptors and interact weakly with the graphene lattice. However, molecules that directly bind on a graphene surface form additional scattering centers, resulting in a change of the mobility of charge carriers.[22] Additionally, practical sensor designs also take into account the changes in interfacial capacitance upon molecules adsorption.[23]

*1.1.3 Sensing with GFETs of high carrier mobility*

The change of the electrical current $\Delta I_{sd}$ resulting from the minute field-effect induced – for example – by the interaction of a biochemical molecule carrying an electron charge, defines the sensing response $S = \Delta I_{sd}/N$. According to Equation (1), $S$ is therefore proportional to the mobility $\mu$ of graphene. With other parameters equal (especially the electrical noise performance), a higher sensing response $S$ implies a better sensor performance.

Because the performance of GFET sensors depends on the mobility $\mu$, the use and integration of high quality graphene into devices is fundamental. To achieve high-quality pristine monolayer or few layer graphene sheets, the most commonly used method is the micromechanical cleavage of graphite with adhesive tape.[9] This so-called 'scotch tape' technique involves splitting few layers of graphene from multi-layered graphite, after which the flakes are pressed and 'dry-deposited' onto a silicon wafer. Compared to graphene synthesized using other methods, micromechanical

cleavage yields graphene with higher mobility and lower intrinsic electrical noise, primarily because fewer structural defects are introduced upon preparation.[24] Generally, for exfoliated graphene on $SiO_2$/Si wafers, mobilities on the order of ~3,000-15,000 $cm^2\ V^{-1}\ s^{-1}$ are reported,[25] which is more than one order of magnitude higher than those of silicon materials (~100-1,500 $cm^2\ V^{-1}\ s^{-1}$).[26] The mobilities of the first graphene-based gas sensor devices were ~5,000 $cm^2\ V^{-1}\ s^{-1}$.[27] Nowadays, at room temperature, carrier mobility up to 100,000-197,600 $cm^2\ V^{-1}\ s^{-1}$, can be achieved by encapsulating graphene in boron nitride (BN),[28] providing unprecedented possibilities for sensing applications. The fact that this idea has only been realized very recently (with h-BN capped $MoS_2$[29]) is not a surprise: groups that work on high quality BN coated graphene samples, very often focus on cryogenic measurements of the physics of the 2D electron gases in graphene rather than its biological sensing applications; moreover, the fabrication methods are very delicate (it is not yet trivial to achieve an ideal interface) and the lack of scalability is still an important drawback.[28a]

Despite all the impressive achievements in the electrical performances of graphene devices, the reproducibility and homogeneity of sample preparation and the relatively small size (on micrometer scale) represent the bottleneck for using exfoliated graphene for practical applications. Larger sheets of few-layer or monolayer graphene can now be directly synthesized via chemical vapor deposition (CVD) on nickel or copper substrates[30] with mobilities rivalling the ones of exfoliated samples.[31] For samples placed on $SiO_2$/Si wafers, mobilities on the order of ~1,000-10,000 $cm^2\ V^{-1}\ s^{-1}$ are now routinely observed and regarded as the standard for graphene transistor products for sensing applications.[32] The electronic performances of CVD graphene[33] can be significantly enhanced by growing single-crystal graphene free of grain boundaries[34] and by using a BN substrate similarly to exfoliated graphene, with which mobility up to ~50,000-350,000 $cm^2\ V^{-1}\ s^{-1}$ can be achieved.[35] These mobility numbers are rivaling those of exfoliated samples, making the CVD process ideal for large-area synthesis of high-quality and uniform graphene for sensing applications.

### *1.1.4 Electrical noise performances of GFETs*

At low frequencies (100 Hz), the ubiquitous $1/f$ noise, whose power spectral density (PSD) spectrum inversely depends on the frequency $f$,[36] seriously impedes the sensing performances of GFETs.[3a] This low-frequency $1/f$ noise is even more pronounced for devices that are scaled down to nanometer dimensions, where the channel current becomes more prone to fluctuations due to, particularly, interface and surface trap states.[37] It is the level of these unwanted fluctuations (along with

the sensing response *S*) that determines the ultimate detection limit of GFET sensors. The 1/*f* noise of graphene mono-layers supported on a substrate is comparable to that of bulk semiconductors (including Si).[38] For freestanding or bilayer graphene, however, the 1/*f* noise was found to be one order of magnitude lower through the effective screening of potential fluctuations from external charged impurities (for example, oxide traps or interface states).[3b, 38] The fact that graphene

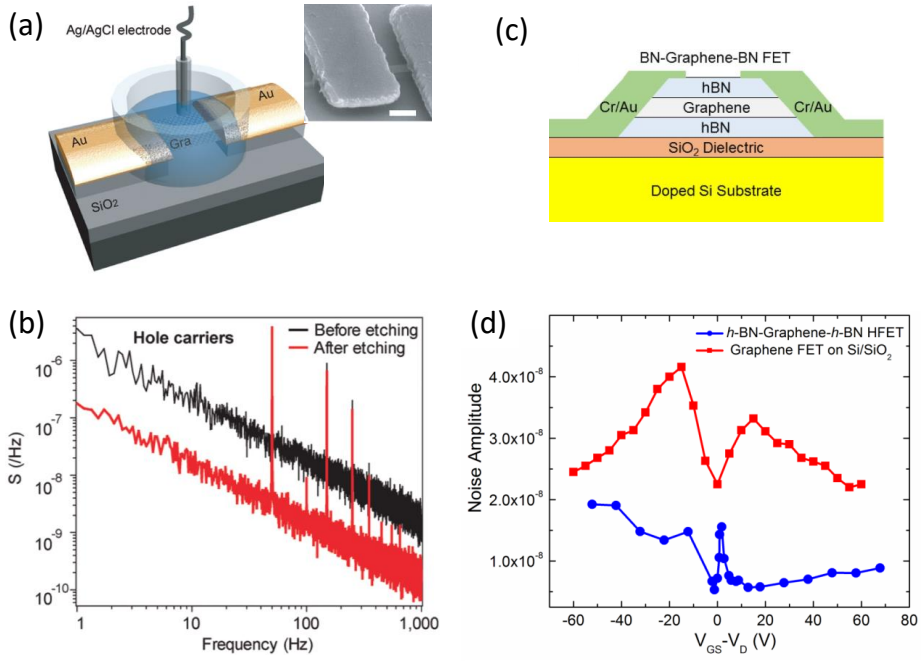


**Figure 1.3 Noise performance of graphene.** a) Schematic representation of the experimental setup where a single-layer graphene is supported in solution by Cr/Au contacts to bridge a trench in the oxide. The inset shows an SEM image of a suspended graphene device. Scale bar is 0.5 μm. b) Comparison of graphene's noise power spectra in the linear operating modes with holes as carriers before (black) and after suspension of the graphene layer (red). The red/black spikes are due to 50 Hz noise coupled from the power lines.[3b] c) Schematics of BN-graphene-BN FET. d) Noise amplitude as a function of the gate voltage for both BN-graphene-BN FET (in blue) and conventional non-encapsulated GFET on $Si/SiO_2$ wafer (in red).[39]

possesses both superior mobility and noise performances, gives it a better signal-to-noise ratio (SNR) as advocated from time to time by literature, reporting graphene based sensors with superior performances compared to their Si based counterpart devices.[40] Figure 1.3b compares the noise performances of a GFET device supported by a $SiO_2/Si$ substrate and its counterpart after suspending the graphene monolayer by etching the underlying $SiO_2$ substrate (Figure 1.3a).[3b] The large noise suppression

was mainly attributed to the removal of any external trap states in the supported $SiO_2$ substrate since the $1/f$ noise in graphene devices is a surface phenomenon.[41]

Similarly, defects in the graphene are another source of noise. For example, the permanent oxygen-based defects contained in graphene oxide (GO) or reduced graphene oxide (rGO) – introduced by over-oxidation (for GO) or incomplete removal of oxygen groups (for rGO) – lead to inferior electrical quality (i.e., degradation in the mobility and noise performance) compared to scotch-tape or CVD graphene.[42] Interestingly, environmental exposure and ageing of graphene devices also increase the level of noise, suggesting that a proper capping layer or surface functionalization may circumvent an increase of noise.[43] Indeed, by encapsulating a single layer graphene between two layers of hexagonal boron nitride (h-BN, as shown in Figure 1.3c), the noise spectral density normalized to the channel area (blue dots, Figure 1.3d) can be suppressed up to one order of magnitude lower compared to non-encapsulated devices on $Si/SiO_2$ (red dots, Figure 1.3d).[39] In the case of silicon FET, the functionalization of the sensor channel (in this case a silicon nanowire buried in a $SiO_2$ dielectric) with 3-aminopropyl-triethoxysilane (APTES) yields better noise performances (up to 60 times), presumably due to the passivation of the oxide traps and interface states at the sensor surface.[44] On the contrary, for carbon nanotubes, a two-level random telegraphic noise (RTN) was reported and ascribed to a single probe molecule (more precisely, the binding and unbinding of charged target molecules at its active sites), which was covalently bound to a defect in the carbon nanotube sidewall.[45] A suppression of the RTN was observed in high ionic strength buffer solutions (ionic screening) and for high gate potentials (when the target molecules are repelled from the nanotube). The influence of surface functionalization on the noise performances of liquid-gated GFETs has not yet been systematically studied. As previously discussed, with other parameters equal (especially the electrical noise performance), a higher mobility implies a better sensor performance when considering the adsorption of charged molecules. It is of note here that a higher mobility also complies with graphene bearing less defects and impurities, which is in favor of an improved noise performance (although there is still not enough experimental evidences or theories that could directly and unambiguously link the high mobility of GFETs to their noise performances).

## 1.2 Graphene for electrochemical sensing

In electrochemically-gated GFETs, the electrical current is confined transversely in the graphene conductive channel. Any electrochemical current vertically flowing between the graphene channel and the liquid gate (through the electrolyte solution), is regarded as a spurious signal and limits the performances of gate controlled GFET

devices.[46] This electrochemical current is – however – at the basis of graphene electrochemical (GEC) sensing, which are complementary to FETs.[47] In this regard, it is necessary to understand the construction as well as the working principle of a GEC sensor, in order to fully appreciate the operation of a GFET. Specifically, the sensing principle of a GEC sensor rests on the electrochemical transfer current between the redox active molecules in the solution-phase and graphene surface.

As a single-layered $sp^2$-hybridized carbon material, graphene has the similar atomic surface structure with highly ordered pyrolytic graphite (HOPG), a classical electrode material for electrochemistry related fundamental studies and applications. However, one of the disadvantages for HOPG is its low reproducibility of the electrode surface due to the abundant edge planes. In contrast, high-quality and homogenous graphene presents a more reproducible surface morphology and chemistry. Moreover, the extraordinarily high mobility and other assets like large specific surface area (2630 $m^2\ g^{-1}$)[48] and large potential window in aqueous media concordantly prepare graphene for electroanalytical and electrocatalytic applications with high sensitivity and stability.

### *1.2.1 The electrochemical activity of graphene*

In electrochemistry, the electron is transferred between the redox molecules and the electrode, whose Fermi level can be tuned through the applied potential. The electron transfer process occurs when the electrochemical potential of the electrode (the Fermi level) is properly aligned with the HOMO/LUMO level of the redox molecules. For instance, the reduction reaction occurs when the electrons flow from the graphene surface to the LUMO orbital of the oxidative molecules. Given a specific redox system, the kinetics of electron transfer (reflected by the heterogeneous electron transfer rate $k^o$) is expected to be closely related to the DOS of graphene. As an important electrode parameter, the DOS at certain energy level defines how many states are available to be occupied by the electrons. Normally a higher DOS, which is determined by the electronic structure of an electrode, improves the possibility of electron transfer between the electrode and the redox systems near its surface.[49] A low DOS at the Fermi level (also illustrated in Figure 1.1c) is general for an infinite pristine graphene sheet.[50]

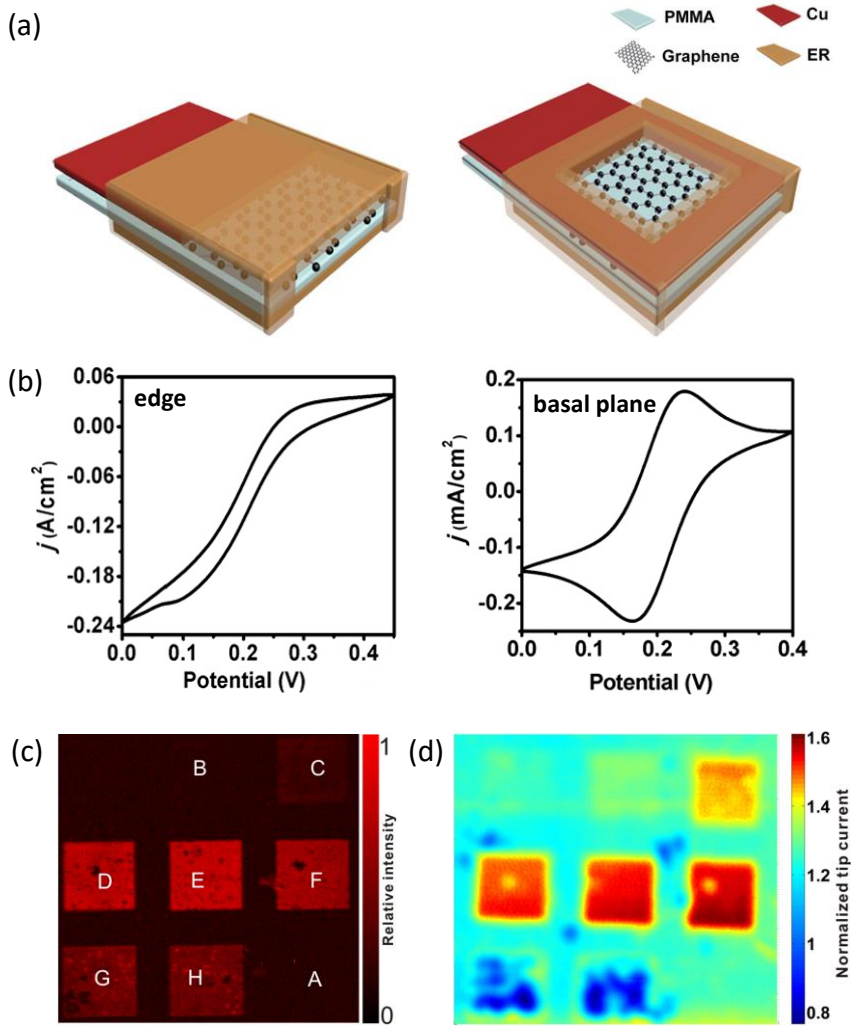


**Figure 1.4 The electrochemical activity of graphene. a)** An illustration of edge-based (left) and basal plane-based (right) CVD graphene. Epoxy resin (ER), a non-conducting pinhole-free polymer, is employed here to coat graphene and only expose the surface of interest. **b)** Cyclic voltammetry studies demonstrated that the current density on edge electrode (0.11 A $cm^{-2}$) is 500 times higher than that on the basal plane one (2.2 × $10^{-4}$ A $cm^{-2}$).[51] **c)** Raman mapping of the D band of the defective graphene patterns (light squares) induced by $Ar^{+}$ irradiation. Window size: 500 μm by 500 μm. **d)** Scanning electrochemical microscopy (SECM) of the same defective graphene patterns with a tip potential of 0.4 V and a substrate potential of 0.11 V. Window size: 500 μm by 500 μm. Square F with medium defect density as tested by Raman spectroscopy exhibits the highest electrochemical activity.[52]

Similarly to GFETs, the GEC uses the surface of graphene as the major sensing element. Until now, the majority of GECs uses graphene dispersions (usually nanosheets of chemically functionalized graphene) deposited on conductive

electrodes.[53] These graphene dispersions with large surface to volume ratio – in contrast with mono- or bilayer graphene sheets employed in GFETs – contain more defective areas. These defects enhance the density of electronic states (DOS) of graphene dispersions, which favors the electron transfer between the graphene materials and the redox molecules, and thus yielding a higher sensitivity.[50] For example, reduced graphene nanowalls (rGNW) with large amount of sharp edges have been deposited vertically via electrophoresis on a graphite electrode to detect double-stranded DNA (dsDNA) with an impressively wide detection concentration range of 0.1 fM – 10 mM.[53b]

The sensitivity of the abovementioned GEC sensors resides in the defects of graphene. Functionalization of these defects with electrochemical catalysts lead to further improved sensitivity and selectivity for the detection of a wide range of molecules, namely glucose,[54] cholesterol,[55] DNA,[56] proteins,[57] and even living cells.[58] To functionalize graphene, most typical catalysts are composed of enzymes,[59] metal nanoparticles,[60] and polymers,[61] to name a few. Advantageously, covalent functionalization often results in dramatically enhanced DOS in graphene facilitating higher electron transfer rate.[50] Non-covalent functionalization, however, has the advantage to retain the excellent electrical properties of graphene, and, to a certain extent, limit the possible charge transfer across the interface, and thus favoring the GFET sensors. Drop-casting deposition[56d] is one of the most widely adopted methodologies to fabricate GEC sensors with functionalized graphene dispersions. Such graphene dispersions, however, usually contain a mixture of mono-, bi-, few layer graphene flakes with uncontrolled and even unknown defect, impurities, or chemical functionalities. In order to unambiguously address the electrochemical properties of graphene, the difference in the electrochemical activity of the edge and the basal plane of graphene have been carefully studied (Figure 1.4a).[51] Graphene edges (with current density j = 0.11 A $cm^{-2}$) exhibit a faster electron transfer than the basal plane (j = $2.2\times10^{-4}$ A $cm^{-2}$), though convergent diffusion induced a faster mass transport can contribute to a higher current density for edges (Figure 1.4b). Previous studies carried out on clean graphene monolayer with a well-defined surface area,[62] on free-standing graphene samples over a nanopore,[63] and on graphene and graphite step edges using scanning electrochemical microscopy (SECM),[52, 64] confirmed this trend that edges are electrochemically more active than the basal plane.[65] In combination with Raman spectroscopy (Figure 1.4c), SECM is able to quantitatively correlate the defect density of graphene with its localized electrochemical activity (Figure 1.4d),[52] providing new possibilities to systematically study the electrochemical properties of graphene. The correlation indicates that the electrochemical activity first increases with the defect density (in line with earlier

reported higher reactivity for covalent derivatization[66]), and then decreases when 'defective' graphene sheet loses its structure integrity (i.e., presumably when the aromaticity of graphene is totally lost). As a perspective, a GFET sensor can in principle be combined with a GEC sensor as described here in a same device, and thus providing a fully complementary sensing platform to study both the electrostatic charge of the molecules but also the electron transfer during redox reaction at the graphene surface. Such device configuration has already been realized in organic electrochemical transistors with graphene-modified gate electrodes, which was proved to significantly improve the selectivity of the organic electrochemical transistors for dopamine detection.[67]

*1.2.2 Graphene-based electrocatalysis*

Chemical functionalization and defects in graphene endow it with high electrocatalytic activity to various (bio)chemical reactions. Specifically, graphene upon nitrogen (N) doping, referred to as nitrogenated graphene or N-doped graphene, has been considered as alternative catalysts to the traditional noble metal based catalysts for oxygen reduction reaction (ORR).[68] As the cathode reaction in fuel cells, electrochemical ORR is known for its notoriously sluggish kinetics. Therefore, considerable attention have been drawn for the development of cathode catalysts with high activity and/or selectivity to gain more energy.[69] ORR involves multiple steps of reaction and electron transfer, in which the pathway is determined by the catalyst itself and electrolyte solution.[70] In aqueous media, ORR mainly produces water via a four-electron pathway or hydrogen peroxide through a two-step two-electron process. Highly selective ORR with exclusive $2e^-$ or $4e^-$ product is equally desired for practical applications. To obtain a higher catalytic efficiency, tremendous efforts have been devoted to experimentally and theoretically determine the active sites in N-doped carbon materials for ORR catalysis.[71] In particular, positive charge in the carbon atoms adjacent to the doped nitrogen atoms have been suggested to preferentially adsorb $O_2$ molecules. Nevertheless, controversies still remain. For example, there is still a debate on whether pyridinic N (N atom bonded to two carbon atoms) or graphitic N (N atom bonded to three carbon atoms) generates the active sites.[72] On other respect, doubts also arise concerning that N-dopant are not active, or are less active than other doping sites like vacancy defects.[71c, 73] Recently, vacancy defects is proposed to exhibit a higher ORR activity than the pyridinic sites in nitrogenated graphite.[74] In summary, all the above-mentioned contradictions mainly originate from the significantly varied structure and surface chemistry of the studied carbon-based materials. For N-doped graphene, the nanoflakes dispersions can be very inhomogeneous in terms of size and crystallinity, caused by unpredictable chemical or physical reactions. Therefore a more reliable and well-defined N-doped

graphene catalyst is desired to disclose the structure–activity correlations for ORR.

### 1.3 Chemical functionalization of graphene for sensing applications

The main requirements for sensing applications are that the detection is sensitive and selective.[75] However, graphene is intrinsically chemically inert due to its large aromatic $sp^2$ carbon lattice that is free of dangling bonds.[46] The broad sensing potential of graphene can only be unlocked by the introduction of sensitizer (bio)molecules and structures, e.g. various inorganic groups,[42, 76] organic or organometallic molecules,[12, 77] DNAs,[78] proteins,[79] peptides,[58b, 80] nanoparticles,[81] and 2D heterostructure[28b, 28c, 35c, 82]. These molecules are able to respond chemically or physically to their nearby environment, whose responses could then be transduced into an appreciable change in the conductivity of the carbon-based honeycomb scaffold. The introduction of such chemical moieties on the graphene surface or edge is often referred to as graphene functionalization.[83] Chemical functionalization of graphene is commonly achieved using either covalent or non-covalent strategies. The resulting graphene materials contain specific recognition moieties for biochemical sensing, but still share, to a large extent, the same carbon honeycomb backbone and the electrical properties, especially the field effect, of graphene. Typically, covalent approaches modify the graphene surface with various functional (bio)chemical molecules[84] by reacting with the $sp^2$ carbon centers in the aromatic lattice, introducing $sp^3$ centers at the reaction sites. Precautions have to be taken because chemical modification reduces the flatness, but more importantly, destroys the aromaticity of the graphene lattice and renders the modified material inferior in terms of electrical mobility compared to pristine graphene. On the contrary, non-covalent approaches provide the opportunity to functionalize graphene without disrupting its intrinsic aromaticity.[85]

#### *1.3.1 Covalent functionalization*

Covalent chemical modification of graphene allows engineering the properties of graphene to a large extend, particularly with the scope of band gap engineering, surface modification, and bio-interfacing.[83a] Introducing atomic hydrogen or fluorine into the honeycomb scaffold, reveals the possibility to continuously transform this highly conductive zero-band gap semimetal into an insulator known as graphane[76a] (Figure 1.5a) or 2D Teflon,[76b, 76c] as initially proposed by the Manchester group. Regarding sensing applications, calculations showed that (partially) hydrogenated graphene has a high affinity for $NO_2$;[86] while graphane doped with Li adatoms was predicted to be sensitive to $H_2S$ and $NH_3$.[87] Moreover, the reduced carrier mobility of highly hydrogenated graphene is still sufficient for sensor applications.[88]

Fluorographene, on the other hand, was applied for the detection of ammonia[89] and ascorbic acid and uric acid.[90] The fluorine-enriched material could also be further functionalized with thiol groups for genosensing.[91] Underlying mechanisms and selectivity of the sensor are still under debate.

Separately, graphene sheets are now routinely covalently modified with oxygen functional groups (e.g. carboxyl, hydroxyl and epoxy moieties, see also Figure 1.5b) by using oxidative reactions, forming graphene oxide (GO), a material known since the early 1960s.[92] The synthetic process consists in dispersing graphite into stable single layer GO and is suitable for large scale production of dispersible single layer graphene using a thermal or chemical reduction step. The resulting material is often referred to as reduced GO, or rGO.[93] Remarkably, when used as an active sensing electrode, GO and rGO usually show improved sensing responses, presumably due to the large concentration of defects compared to near defect-free single layer graphene obtained via mechanical exfoliation of graphite.[42, 94] One of the first works on rGO as an active material for high-performance molecular sensing describes a conductance change of the rGO networks upon exposure to trace levels of vapor (including three main classes of chemical-warfare agents and an explosive at parts-per-billion concentrations).[42] It was shown that the optimal defect density should balance the gains in the sensor response against the rapid degradation in low frequency $1/f$ noise due to the increased density of defects.[42] The difficulties in controlling the density of the defect as well as the lack of knowledge on the nature of the defect, however, represents significant limitations for utilizing GO or rGO for sensing applications. Reactive oxygen-rich groups, inherently present on rGO, can be exploited to synthetically conjugate the material with various chemical or biological groups.[84] A viable synthetic strategy is depicted in Figure 1.5b: a GO-polyethylene glycol dispersion (i.e., PEGylated GO) was prepared; the hydrophilic six-armed PEG-$NH_2$ could then be labelled by conjugating an antibody (for potential antibody-antigen detection[84]).

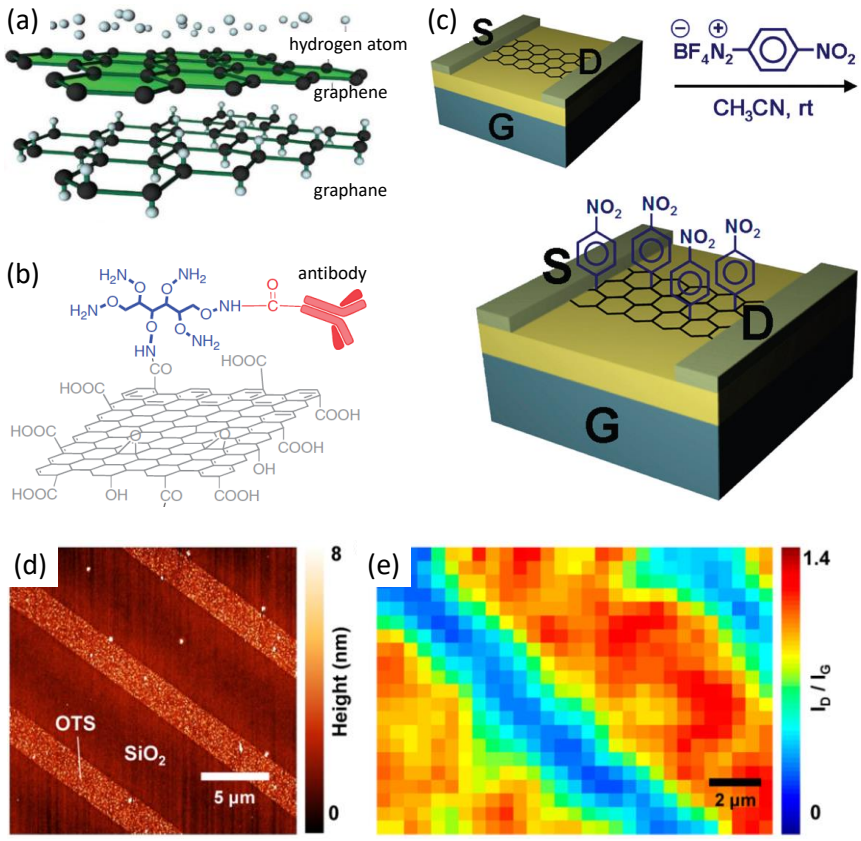


**Figure 1.5 Covalent functionalization of graphene.** a) Chemical modification of a graphene layer (in green) with cold plasma hydrogen atoms produces graphane.[76a] b) Bioconjugation of PEGylated GO with antibody.[92] c) Schematic of the chemical functionalization of a GFET devices with 4-nitrobenzene diazonium tetrafluoroborate (4-NBD).[95] d) AFM image of octadecyltrichlorosilane (OTS) lines patterned on $SiO_2$ surface. e) Raman mapping of $I_D/I_G$ for graphene after 4-NBD reactions: 10mM 4-NBD in aqueous solution with 0.5 wt% sodium dodecyl sulfate (SDS) at 35°C for 1.5 h.[96]

Hydrogenated graphene, fluorinated graphene (or halogenated graphene[97] in general), and GO (or rGO) are the few examples of materials that resulted from covalent modification of the graphene scaffold. Instead of providing an extensive list of the methods available to induce such modifications, more focus will be on discussing a grafting strategy, frequently applied to covalently attach chemical moieties to graphene surface (or edges) usually proceeds via free-radical reactions.[65, 66b, 83a, 96, 98] Graphene grafting uses alkyl or aryl diazonium salts as grafting agents, where the diazonium salt precursor is first chemically or electrochemically reduced (liberating nitrogen gas), to form a reactive alkyl or aryl radical that reacts with the aromatic system of the graphene sheet (the conductive channel of the transistor

device fabricated on a 200 nm $SiO_2$/highly doped Si substrate as shown in Figure 1.5c).[95] The disruption of the aromatic system by transformation of carbon atoms from $sp^2$ to $sp^3$ hybridization results in a remarkable decrease in graphene conductivity, which can be controlled by reaction time. The reaction efficiency depends on several parameters: the number of graphene layers,[66b] the electrostatic environment,[98c] and the defect density on the graphene surface.[98d] A previous study exploited the graphene reactivity, induced by electrostatic charge doping on different substrates using reactivity imprint lithography (RIL).[98c] The RIL technique made use of a polydimethylsiloxane (PDMS) stamp to pattern octadecyltrichlorosilane (OTS) lines on a $SiO_2$/Si substrate (Figure 1.5d). During the electrografting of graphene with 4-nitrobenzene diazonium tetrafluoroborate (4-NBD),[96] bare $SiO_2$-supported graphene showed a stronger reactivity with the diazonium salt than graphene resting on OTS-protected $SiO_2$ (Figure 1.5e). OTS increases the distance between the graphene sheet and the charged impurities in the $SiO_2$ substrate, rendering the portion of graphene resting on it less reactive to the 4-NBD.[98c] Similarly, in case of GO (or rGO), grafting chemistries are best represented by localized reactivity of the carboxyl, carbonyl, and other oxygen-containing groups by substitution reactions.[98d]

*1.3.2 Non-covalent functionalization*

Non-covalent functionalization have the major advantage of fully preserving the graphene lattice (i.e., the aromaticity), and thus the electrical performances. In addition, non-covalent bond can also be quite strong. For example, the π–π interactions of graphene-benzene and naphthalene result in a considerable binding energy of almost 0.1 eV per carbon atom; consistently, the binding energy of graphene-TTP (tetraphenylporphyrin) was calculated to be 3.2 eV, i.e., ≈90% of a typical C-C covalent binding energy (≈3.6 eV).[99] Given the aforementioned advantages, it is a common approach to anchor a molecule onto the graphene surface using an aromatic linker group via noncovalent bonds with excellent sensing performance in aqueous solutions.[83a] Still, it is of note here that non-covalent functionalization is expected to be less compatible with long term usage, at least if compared to stronger covalent functionalization (although the covalent modifications of graphene inevitably lead to a severe degradation in the electrical properties). Nevertheless, non-covalent functionalization could also be an asset if the sensor surface has to be regenerated, for example, for recycling the sensor devices.

In general, non-covalent graphene functionalization approaches can be classified based on their corresponding intermolecular interactions, including π-π or hydrophobic stacking, electrostatic interaction, and van der Waals interaction.[83a] The self-assembly process of these molecules on the surface of graphene could be

highly controlled and accurately characterized in favor of actual sensor design.[83] For example, Figure 1.6a shows a scanning tunneling microscopy (STM) image of well-ordered aromatic perylene-3,4,9,10-tetracarboxylic-3,4,9,10-dianhydride (PTCDA) molecules on graphene (as indicated by the **a** and **b** vectors), where π-π interaction are the driving force of the self-assembly.[77b] The perylene-based monolayer is stable and robust even when exposed to ambient conditions. π-π or hydrophobic interactions between aromatic surface and nucleic acid moieties can also facilitate the decoration of graphene surface with single-stranded DNA (ssDNA) as shown in Figure 1.6b (right panel, highly oriented pyrolytic graphite (HOPG) was applied in this case).[100] This strong non-specific ssDNA adsorption can be avoided by first self-assembling a monolayer of pyrene ethylene glycol, thus rendering the surface of graphene hydrophilic and preventing ssDNA adsorption via hydrophobic interactions (left panel, Figure 1.6b). Besides DNA, proteins[79] or peptides[80a, 80b] containing aromatic moieties could also self-assemble on a graphene scaffold. As illustrated in Figure 1.6c, the incubation of graphene with the peptides resulted in the formation of a uniform mesh-like layer whilst silicon oxide surface was unaffected. This indicates that the adsorption occurred specifically on graphene.[80b]

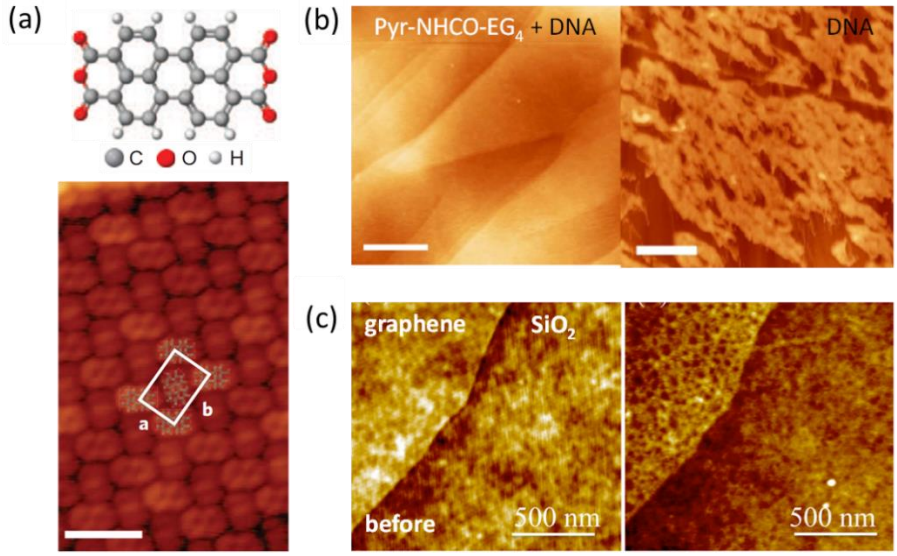


**Figure 1.6 Non-covalent functionalization of graphene**. a) STM image of a self-assembled monolayer of an aromatic molecule (perylene-3,4,9,10-tetracarboxylic-3,4,9,10-dianhydride, PTCDA) (gas-phase deposition) on a graphene surface (scale bar is 3 nm). Upper panel: molecular structure of PTCDA.[77b] b) Left panel: AFM of highly oriented pyrolytic graphite (HOPG) incubated for 5 min with a solution of 3 M KCl and 8 M urea and rinsed with ultrapure water (scale bar is 200 nm). Right panel: HOPG incubated for 5 min with single-stranded M13 DNA (10 ng $\mu l^{-1}$) in the same buffer (scale bar is 200 nm).[100] c) AFM topographic image of graphene before (left panel) and after (right panel) incubation with the peptide.[80b]

Electrostatic interaction is another driving force of the non-covalent assembly. For instance, voltage-biased graphene can act as an electrophoretic electrode for immobilization of charged molecules. The subsequent detection of complementary analysts can be achieved by using the same graphene transistor devices.[17, 77h, 101]

As suggested by Geim and co-workers,[82] weak van der Waals-like interaction between layers could be exploited to sandwich (a process called 'encapsulation') graphene with other 2D layers of, e.g. $MoS_2$, mica, or hexagonal boron nitride (h-BN). This innovative technique allows the formation of unprecedented multilayer heterostructures that may be used in devices with adjustable and astonishing electronic properties. For example, by encapsulating graphene in a h-BN stacking layer, researchers managed to obtain very high electric performances GFETs, including an exceptionally high carrier mobility of 140,000 $cm^2\ V^{-1}\ s^{-1}$ at room temperature, which is close to the theoretical limit as imposed by acoustic phonon scattering. This extremely high mobility could be ascribed to very clean interfaces above and below graphene and effective screening of all the defects.[28a] Very recently, even higher mobilities, up to a staggering 197,600 $cm^2\ V^{-1}\ s^{-1}$ and 350,000 $cm^2\ V^{-1}\ s^{-1}$, have been observed for hBN-sandwiched graphene samples.[28c, 35c] One could also explore various 2D crystals as active sensing elements, $MoS_2$ or h-BN capped $MoS_2$,[29, 102] for instance. Please note that even in a stack such as encapsulated graphene, the encapsulating layers can be functionalized in the quest of sensing (with the requirement that the encapsulating layer is sufficiently thin).

As previously discussed, chemical functionalization is essential for unlocking the sensing potential of graphene surface, but important is also to realize that chemical functionalization also plays a critical role in passivating the surface of graphene. Surface passivation against unwanted non-specific binding (pyrene ethylene glycol to prevent any hydrophobic interactions,[100] for example) is crucial to achieve very low detection limits in the presence of high ionic background levels and to avoid false positives when complex biological samples are assayed.[103]

Importantly, the transfer of large and clean (and crack- and fold-free) graphene sheets is still a critical challenge. Long chain polymers including poly(methyl methacrylate) (PMMA) – conventionally used for transferring two-dimensional materials – irreversibly adsorb on the graphene surface, yielding a range of contaminations with unwanted chemical functions.[104] It is therefore a necessity to take into account the influences of these possible polymer residues as they impede the functionalization of the graphene surface (which is actually not always discussed, nor clarified in the literature). There is therefore also a large demand for decent polymer-free transfer methods.[105]

## 1.4 Aims and outline

Graphene as a 2D surface with unique band structure, extraordinary high mobility and versatile (electro-)chemical reactivity has great potential and advantages for sensing applications. The thesis aims to understand at a fundamental level the electrical, electrochemical and mechanical properties of graphene surface upon chemical modifications, and thus using these properties for sensing applications.

In chapter 2, the electrical transport properties and electrochemical kinetics of graphene upon hydrogenation are discussed. As the electronic density of states (DOS) is closely related to both the electrical and electrochemical properties, the correlations between the DOS, quantum capacitance and the heterogeneous electron transfer rate were established and discussed. Furthermore, by correlating the charged impurity density and the density of hydrogenated defects, hydrogenation treatment via the mild hydrogen plasma was found to clean the graphene lattice by removing airborne hydrocarbons.

In Chapter 3, nitrogen atoms were incorporated into graphene lattice using an ammonia plasma to study the electrocatalysis of oxygen reduction reaction (ORR). Nitrogen doping sites in graphene, as generally believed to be the active sites for ORR, were found not to be responsible for the activity improvement. Instead, oxygen containing groups which coexist with the nitrogen dopants at graphene surface are at the origin of the enhanced ORR activity.

The 2D nature of graphene makes its surface chemistry very sensitive to the environment. Chapter 4 reveals the enhanced surface cleanliness of graphene using hydrogenation treatment. Characterization by multiscale surface spectroscopy techniques showed that hydrogenation is able to remove hydrocarbons contaminations from the surface of graphene. As compared to pristine graphene, hydrogenation induced more water adsorption that forms a layer protecting the graphene surface from airborne contaminants.

Surface chemistry modification not only alters the electrical and electrochemical properties, but also exerts significant impact on the mechanical properties of graphene. In Chapter 5, the mechanical strength of centimeter-scale graphene via a biaxial compression method is investigated. When graphene floats on water, the natural perturbations of graphene remain untouched, which provides a unique strategy to evaluate the in-plane stiffness of graphene. In the framework of the anharmonic coupling the stretching and flexural modes, the mechanical stiffness of graphene is proven to be very sensitive to lattice defects including hydrogenation and

vacancy.

Hydrogenated and nitrogenated graphene are used for field effect detection of a range of gas in Chapter 6. Compared to pristine graphene, the chemically modified graphene exhibits p-doping behaviors and improved sensing responses with low selectivity. Upon continuous gas detection, the graphene devices tend to show saturated and then decreased responses due to the reduction of active adsorption sites caused by trapped gas molecules. Further exploration suggests that p-doping in the modified graphene is positively correlated to the enhanced sensitivity of graphene to gas detection.

## 1.6 References


[1] A. K. Geim, K. S. Novoselov, *Nat. Mater.* **2007**, 6, 183.

[2] Y. Wu, D. B. Farmer, F. Xia, P. Avouris, *Proc. IEEE* **2013**, 101, 1620.

[3] a) A. A. Balandin, *Nat. Nanotechnol.* **2013**, 8, 549; b) Z. Cheng, Q. Li, Z. Li, Q. Zhou, Y. Fang, *Nano Lett.* **2010**, 10, 1864.

[4] Q. He, S. Wu, Z. Yin, H. Zhang, *Chem. Sci.* **2012**, 3, 1764.

[5] S. Wu, Q. He, C. Tan, Y. Wang, H. Zhang, *Small* **2013**, 9, 1160.

[6] C. T. Lin, P. T. K. Loan, T. Y. Chen, K. K. Liu, C. H. Chen, K. H. Wei, L. J. Li, *Adv. Funct. Mater.* **2013**, 23, 2301.

[7] S. Chen, Z.-B. Zhang, L. Ma, P. Ahlberg, X. Gao, Z. Qiu, D. Wu, W. Ren, H.-M. Cheng, S.-L. Zhang, *Appl. Phys. Lett.* **2012**, 101, 154106.

[8] W. Fu, C. Nef, A. Tarasov, M. Wipf, R. Stoop, O. Knopfmacher, M. Weiss, M. Calame, C. Schönenberger, *Nanoscale* **2013**, 5, 12104.

[9] K. S. Novoselov, A. K. Geim, S. V. Morozov, D. Jiang, Y. Zhang, S. V. Dubonos, I. V. Grigorieva, A. A. Firsov, *Science* **2004**, 306, 666.

[10] a) F. Schedin, A. Geim, S. Morozov, E. Hill, P. Blake, M. Katsnelson, K. Novoselov, *Nat. Mater.* **2007**, 6, 652; b) Y. Ohno, K. Maehashi, K. Matsumoto, presented at Micro-and Nanotechnology Sensors, Systems, and Applications III **2011**; c) I. Heller, S. Chatoor, J. Männik, M. A. Zevenbergen, C. Dekker, S. G. Lemay, *J. Am. Chem. Soc.* **2010**, 132, 17149.

[11] Y. Dan, Y. Lu, N. J. Kybert, Z. Luo, A. C. Johnson, *Nano Lett.* **2009**, 9, 1472.

[12] W. Fu, C. Nef, A. Tarasov, M. Wipf, R. Stoop, O. Knopfmacher, M. Weiss, M. Calame, C. Schonenberger, *Nanoscale* **2013**, 5, 12104.

[13] a) J. L. Xia, F. Chen, J. H. Li, N. J. Tao, *Nat. Nanotechnol.* **2009**, 4, 505; b) S. Luryi, *Appl. Phys. Lett.* **1988**, 52, 501.

[14] J. O. Bockris, E. Gileadi, K. Muller, *J. Chem. Phys.* **1966**, 44, 1445.

[15] V. M. Aguilella, J. Pellicer, M. Aguilella-Arzo, *Langmuir* **1999**, 15, 6156.

[16] a) P. Bergveld, *Sensor. Actuat. B* **2003**, 88, 1; b) P. Bergveld, *IEEE Trans. Biomed. Eng.* **1970**, Bm17, 70.

[17] G. Y. Xu, J. Abbott, L. Qin, K. Y. M. Yeung, Y. Song, H. Yoon, J. Kong, D. Ham, *Nat. Commun.* **2014**, 5, 4866.

[18] J. J. Gooding, *Small* **2006**, 2, 313.

[19] X. P. A. Gao, G. F. Zheng, C. M. Lieber, *Nano Lett.* **2010**, 10, 547.

[20] G. S. Kulkarni, Z. H. Zhong, *Nano Lett.* **2012**, 12, 719.

[21] K. S. Chang, C. C. Chen, J. T. Sheu, Y. K. Li, *Sensor. Actuat. B* **2009**, 138, 148.

[22] C. T. Lin, P. T. K. Loan, T. Y. Chen, K. K. Liu, C. H. Chen, K. H. Wei, L. J. Li, *Adv. Funct. Mater.* **2013**, 23, 2301.

[23] S. Chen, Z. B. Zhang, L. P. Ma, P. Ahlberg, X. D. Gao, Z. J. Qiu, D. P. Wu, W. C. Ren, H. M. Cheng, S. L. Zhang, *Appl. Phys. Lett.* **2012**, 101, 154106.

[24] V. Singh, D. Joung, L. Zhai, S. Das, S. I. Khondaker, S. Seal, *Prog. Mater. Sci.* **2011**, 56, 1178.

[25] a) E. W. Hill, A. Vijayaragahvan, K. Novoselov, *IEEE Sens. J.* **2011**, 11, 3161; b) H. C. Cheng, R. J. Shiue, C. C. Tsai, W. H. Wang, Y. T. Chen, *ACS Nano* **2011**, 5, 2051.

[26] E. Stern, J. F. Klemic, D. A. Routenberg, P. N. Wyrembak, D. B. Turner-Evans, A. D. Hamilton, D. A. LaVan, T. M. Fahmy, M. A. Reed, *Nature* **2007**, 445, 519.

[27] F. Schedin, A. K. Geim, S. V. Morozov, E. W. Hill, P. Blake, M. I. Katsnelson, K. S. Novoselov, *Nat. Mater.* **2007**, 6, 652.

[28] a) L. Wang, I. Meric, P. Y. Huang, Q. Gao, Y. Gao, H. Tran, T. Taniguchi, K. Watanabe, L. M. Campos, D. A. Muller, J. Guo, P. Kim, J. Hone, K. L. Shepard, C. R. Dean, *Science* **2013**, 342, 614; b) D. H. Tien, J.-Y. Park, K. B. Kim, N. Lee, T. Choi, P. Kim, T. Taniguchi, K. Watanabe, Y. Seo, *ACS Appl. Mater. Interfaces* **2016**, 8, 3072; c) G. Auton, J. Zhang, R. K. Kumar, H. Wang, X. Zhang, Q. Wang, E. Hill, A. Song, *Nat. Commun.* **2016**, 7, 11670.

[29] G. Liu, S. L. Rumyantsev, C. Jiang, M. S. Shur, A. A. Balandin, *IEEE Electron Device Lett.* **2015**, 36, 1202.

[30] a) K. S. Kim, Y. Zhao, H. Jang, S. Y. Lee, J. M. Kim, K. S. Kim, J. H. Ahn, P. Kim, J. Y. Choi, B. H. Hong, *Nature* **2009**, 457, 706; b) X. S. Li, W. W. Cai, J. H. An, S. Kim, J. Nah, D. X. Yang, R. Piner, A. Velamakanni, I. Jung, E. Tutuc, S. K. Banerjee, L. Colombo, R. S. Ruoff, *Science* **2009**, 324, 1312.

[31] A. W. Tsen, L. Brown, M. P. Levendorf, F. Ghahari, P. Y. Huang, R. W. Havener, C. S. Ruiz-Vargas, D. A. Muller, P. Kim, J. Park, *Science* **2012**, 336, 1143.

[32] a) *SIGMA-ALDRICH*, Graphene field effect transistor chip, **2016,** http://www.sigmaaldrich.com/technical-documents/articles/materials-science/graphene-field-effect-transistors.html#newMaterials, DOI: http://www.sigmaaldrich.com/catalog/product/aldrich/803995?lang=en&region=NL; b) *L. BGT Materials Limited*, Grat-FET™, **2015,** http://bgtmaterials.com/uploads/BGT%20Materials%20Limited_Grat%20FET_Data%20Sheet%2017Jun2015.pdf.

[33] H. S. Song, S. L. Li, H. Miyazaki, S. Sato, K. Hayashi, A. Yamada, N. Yokoyama, K. Tsukagoshi, *Sci. Rep.* **2012**, 2, 337.

[34] a) Z. Yan, Z. W. Peng, J. M. Tour, *Acc. Chem. Res.* **2014**, 47, 1327; b) T. R. Wu, X. F. Zhang, Q. H. Yuan, J. C. Xue, G. Y. Lu, Z. H. Liu, H. S. Wang, H. M. Wang, F. Ding, Q. K. Yu, X. M. Xie, M. H. Jiang, *Nat. Mater.* **2016**, 15, 43.

[35] a) K. H. Lee, H. J. Shin, J. Lee, I. Y. Lee, G. H. Kim, J. Y. Choi, S. W. Kim, *Nano Lett.* **2012**, 12, 714; b) N. Petrone, C. R. Dean, I. Meric, A. M. van der Zande, P. Y. Huang, L. Wang, D. Muller, K. L. Shepard, J. Hone, *Nano Lett.* **2012**, 12, 2751; c) L. Banszerus, M. Schmitz, S. Engels, J. Dauber, M. Oellers, F. Haupt, K. Watanabe, T. Taniguchi, B. Beschoten, C. Stampfer, *Sci Adv* **2015**, 1, e1500222.

[36] F. Hooge, T. Kleinpenning, L. Vandamme, *Rep. Prog. Phys.* **1981**, 44, 479.

[37] a) N. K. Rajan, D. A. Routenberg, M. A. Reed, *Appl. Phys. Lett.* **2011**, 98, 264107; b) G. Liu, S. Rumyantsev, M. S. Shur, A. A. Balandin, *Appl. Phys. Lett.* **2013**, 102, 093111.

[38] Y.-M. Lin, P. Avouris, *Nano Lett.* **2008**, 8, 2119.

[39] M. A. Stolyarov, G. X. Liu, S. L. Rumyantsev, M. Shur, A. A. Balandin, *Appl. Phys. Lett.* **2015**, 107, 023106.

[40] L. H. Hess, M. Seifert, J. A. Garrido, *Proc. IEEE* **2013**, 101, 1780.

[41] G. X. Liu, S. Rumyantsev, M. S. Shur, A. A. Balandin, *Appl. Phys. Lett.* **2013**, 102, 093111.

[42] J. T. Robinson, F. K. Perkins, E. S. Snow, Z. Q. Wei, P. E. Sheehan, *Nano Lett.* **2008**, 8, 3137.

[43] G. Liu, W. Stillman, S. Rumyantsev, Q. Shao, M. Shur, A. A. Balandin, *Appl. Phys. Lett.* **2009**, 95, 033103.

[44] N. K. Rajan, K. Brower, X. X. Duan, M. A. Reed, *Appl. Phys. Lett.* **2014**, 104, 084106.

[45] S. Sorgenfrei, C. Y. Chiu, M. Johnston, C. Nuckolls, K. L. Shepard, *Nano Lett.* **2011**, 11, 3739.

[46] W. Y. Fu, C. Nef, O. Knopfrnacher, A. Tarasov, M. Weiss, M. Calame, C. Schonenberger, *Nano Lett.* **2011**, 11, 3597.

[47] Y. Y. Shao, J. Wang, H. Wu, J. Liu, I. A. Aksay, Y. H. Lin, *Electroanalysis* **2010**, 22, 1027.

[48] M. D. Stoller, S. Park, Y. Zhu, J. An, R. S. Ruoff, *Nano Lett.* **2008**, 8, 3498.

[49] W. J. Royea, T. W. Hamann, B. S. Brunschwig, N. S. Lewis, *J. Phys. Chem. B* **2006**, 110, 19433.

[50] R. L. McCreery, *Chem. Rev.* **2008**, 108, 2646.

[51] W. Yuan, Y. Zhou, Y. Li, C. Li, H. Peng, J. Zhang, Z. Liu, L. Dai, G. Shi, *Sci. Rep.* **2013**, 3, 2248.

[52] J.-H. Zhong, J. Zhang, X. Jin, J.-Y. Liu, Q. Li, M.-H. Li, W. Cai, D.-Y. Wu, D. Zhan, B. Ren, *J. Am. Chem. Soc.* **2014**, 136, 16609.

[53] a) Y. Wang, Y. Shao, D. W. Matson, J. Li, Y. Lin, *ACS Nano* **2010**, 4, 1790; b) O. Akhavan, E. Ghaderi, R. Rahighi, *ACS Nano* **2012**, 6, 2904; c) J. Guo, T. Zhang, C. Hu, L. Fu, *Nanoscale* **2015**, 7, 1290; d) V. Urbanová, F. Karlický, A. Matěj, F. Šembera, Z. Janoušek, J. A. Perman, V. Ranc, K. Čépe, J. Michl, M. Otyepka, *Nanoscale* **2016**, 8, 12134.

[54] a) C. Ruan, W. Shi, H. Jiang, Y. Sun, X. Liu, X. Zhang, Z. Sun, L. Dai, D. Ge, *Sens. Actuators. B* **2013**, 177, 826; b) B. Unnikrishnan, S. Palanisamy, S.-M. Chen, *Biosens. Bioelectron.* **2013**, 39, 70.

[55] S. S. J. Aravind, T. T. Baby, T. Arockiadoss, R. B. Rakhi, S. Ramaprabhu, *Thin Solid Films* **2011**, 519, 5667.

[56] a) Y. Guo, Y. Guo, C. Dong, *Electrochim. Acta* **2013**, 113, 69; b) K.-J. Huang, Y.-J. Liu, H.-B. Wang, T. Gan, Y.-M. Liu, L.-L. Wang, *Sens. Actuators. B* **2014**, 191, 828; c) Y. Ni, P. Wang, H. Song, X. Lin, S. Kokot, *Anal. Chim. Acta* **2014**, 821, 34; d) L. Zhu, L. Luo, Z. Wang, *Biosens. Bioelectron.* **2012**, 35, 507.

[57] a) B. Jin, P. Wang, H. Mao, B. Hu, H. Zhang, Z. Cheng, Z. Wu, X. Bian, C. Jia, F. Jing, *Biosens. Bioelectron.* **2014**, 55, 464; b) F. Liu, K. S. Choi, T. J. Park, S. Y. Lee, T. S. Seo, *BioChip J.* **2011**, 5, 123; c) Z. Wang, F. Li, J. Xia, L. Xia, F. Zhang, S. Bi, G. Shi, Y. Xia, J. Liu, Y. Li, *Biosens. Bioelectron.* **2014b**, 61, 391.

[58] a) Y. Wang, Z. Li, D. Hu, C.-T. Lin, J. Li, Y. Lin, *J. Am. Chem. Soc.* **2010**, 132, 9274; b) L. Feng, Y. Chen, J. Ren, X. Qu, *Biomaterials* **2011**, 32, 2930.

[59] A. Muthurasu, V. Ganesh, *Appl. Biochem. Biotechnol.* **2014**, 174, 945.

[60] a) J. C. Claussen, A. Kumar, D. B. Jaroch, M. H. Khawaja, A. B. Hibbard, D. M. Porterfield, T. S. Fisher, *Adv. Funct. Mater.* **2012**, 22, 3399; b) D. Pan, Y. Gu, H. Lan, Y. Sun, H. Gao, *Anal. Chim. Acta* **2015**, 853, 297; c) Z. Yang, Y. Cao, J. Li, Z. Jian, Y. Zhang, X. Hu, *Anal. Chim. Acta* **2015**, 871, 35.

[61] Y. Yang, M. Kang, S. Fang, M. Wang, L. He, J. Zhao, H. Zhang, Z. Zhang, *Sens. Actuators. B* **2015**, 214, 63.

[62] W. Li, C. Tan, M. A. Lowe, H. D. Abruna, D. C. Ralph, *ACS Nano* **2011**, 5, 2264.

[63] S. Banerjee, J. Shim, J. Rivera, X. Jin, D. Estrada, V. Solovyeva, X. You, J. Pak, E. Pop, N. Aluru, *ACS Nano* **2012**, 7, 834.

[64] a) C. Tan, J. n. Rodríguez-López, J. J. Parks, N. L. Ritzert, D. C. Ralph, H. c. D. Abruña, *ACS Nano* **2012**, 6, 3070; b) N. L. Ritzert, J. Rodríguez-López, C. Tan, H. c. D. Abruña, *Langmuir* **2013**, 29, 1683; c) A. G. Guell, A. S. Cuharuc, Y. R. Kim, G. H. Zhang, S. Y. Tan, N. Ebejer, P. R. Unwin, *ACS Nano* **2015**, 9, 3558.

[65] A. Bellunato, H. Arjmandi Tash, Y. Cesa, G. F. Schneider, *ChemPhysChem* **2016**, 17, 785.

[66] a) R. Sharma, J. H. Baik, C. J. Perera, M. S. Strano, *Nano Lett.* **2010**, 10, 398; b) F. M. Koehler, A. Jacobsen, K. Ensslin, C. Stampfer, W. J. Stark, *Small* **2010**, 6, 1125; c) K. S. Mali, J. Greenwood, J. Adisoejoso, R. Phillipson, S. De Feyter,

*Nanoscale* **2015**, 7, 1566; d) K. Yong-Jin, K. Yuna, N. Konstantin, H. Byung Hee, *2D Mater.* **2015**, 2, 042001; e) A. Criado, M. Melchionna, S. Marchesan, M. Prato, *Angew. Chem. Int. Ed.* **2015**, 54, 10734.

[67] C. Z. Liao, M. Zhang, L. Y. Niu, Z. J. Zheng, F. Yan, *J. Mater. Chem. B* **2014**, 2, 191.

[68] S. K. Singh, K. Takeyasu, J. Nakamura, *Adv. Mater.* **2018**, 31, 1804297.

[69] a) K. Gong, F. Du, Z. Xia, M. Durstock, L. Dai, *Science* **2009**, 323, 760; b) J. Shui, M. Wang, F. Du, L. Dai, *Sci. Adv.* **2015**, 1, e1400129; c) Y. Ito, H. J. Qiu, T. Fujita, Y. Tanabe, K. Tanigaki, M. Chen, *Adv. Mater.* **2014**, 26, 4145; d) L. Qu, Y. Liu, J.-B. Baek, L. Dai, *ACS Nano* **2010**, 4, 1321.

[70] M. Shao, Q. Chang, J.-P. Dodelet, R. Chenitz, *Chem. Rev.* **2016**, 116, 3594.

[71] a) D. Guo, R. Shibuya, C. Akiba, S. Saji, T. Kondo, J. Nakamura, *Science* **2016**, 351, 361; b) H. B. Yang, J. Miao, S.-F. Hung, J. Chen, H. B. Tao, X. Wang, L. Zhang, R. Chen, J. Gao, H. M. Chen, *Sci. Adv.* **2016**, 2, e1501122; c) L. Lai, J. R. Potts, D. Zhan, L. Wang, C. K. Poh, C. Tang, H. Gong, Z. Shen, J. Lin, R. S. Ruoff, *Energy Environ. Sci.* **2012**, 5, 7936; d) T. Wang, Z.-X. Chen, Y.-G. Chen, L.-J. Yang, X.-D. Yang, J.-Y. Ye, H.-P. Xia, Z.-Y. Zhou, S.-G. Sun, *ACS Energy Lett.* **2018**, 3, 986.

[72] a) H.-W. Liang, X. Zhuang, S. Brüller, X. Feng, K. Müllen, *Nat. Commun.* **2014**, 5, 4973; b) W. Ding, Z. Wei, S. Chen, X. Qi, T. Yang, J. Hu, D. Wang, L. J. Wan, S. F. Alvi, L. Li, *Angew. Chem. Int. Ed.* **2013**, 52, 11755.

[73] a) Z. Luo, S. Lim, Z. Tian, J. Shang, L. Lai, B. MacDonald, C. Fu, Z. Shen, T. Yu, J. Lin, *J. Mater. Chem.* **2011**, 21, 8038; b) Y. Jia, L. Zhang, A. Du, G. Gao, J. Chen, X. Yan, C. L. Brown, X. Yao, *Adv. Mater.* **2016**, 28, 9532.

[74] Y. Jia, L. Zhang, L. Zhuang, H. Liu, X. Yan, X. Wang, J. Liu, J. Wang, Y. Zheng, Z. Xiao, *Nat. Catal.* **2019**, 2, 688.

[75] a) A. P. F. Turner, *Chem. Soc. Rev.* **2013**, 42, 3184; b) T. M. H. Lee, *Sensors* **2008**, 8, 5535; c) M. Y. Shen, B. R. Li, Y. K. Li, *Biosens. Bioelectron.* **2014**, 60, 101.

[76] a) D. C. Elias, R. R. Nair, T. M. G. Mohiuddin, S. V. Morozov, P. Blake, M. P. Halsall, A. C. Ferrari, D. W. Boukhvalov, M. I. Katsnelson, A. K. Geim, K. S. Novoselov, *Science* **2009**, 323, 610; b) J. T. Robinson, J. S. Burgess, C. E.

Junkermeier, S. C. Badescu, T. L. Reinecke, F. K. Perkins, M. K. Zalalutdniov, J. W. Baldwin, J. C. Culbertson, P. E. Sheehan, E. S. Snow, *Nano Lett.* **2010**, 10, 3001; c) R. R. Nair, W. C. Ren, R. Jalil, I. Riaz, V. G. Kravets, L. Britnell, P. Blake, F. Schedin, A. S. Mayorov, S. J. Yuan, M. I. Katsnelson, H. M. Cheng, W. Strupinski, L. G. Bulusheva, A. V. Okotrub, I. V. Grigorieva, A. N. Grigorenko, K. S. Novoselov, A. K. Geim, *Small* **2010**, 6, 2877; d) J. S. Burgess, B. R. Matis, J. T. Robinson, F. A. Bulat, F. Keith Perkins, B. H. Houston, J. W. Baldwin, *Carbon* **2011**, 49, 4420; e) F. Withers, M. Dubois, A. K. Savchenko, *Phys. Rev. B* **2010**, 82, 073403; f) K.-I. Ho, C.-H. Huang, J.-H. Liao, W. Zhang, L.-J. Li, C.-S. Lai, C.-Y. Su, *Sci. Rep.* **2014**, 4, 5893; g) X. Zhang, A. Hsu, H. Wang, Y. Song, J. Kong, M. S. Dresselhaus, T. Palacios, *ACS Nano* **2013**, 7, 7262; h) B. Li, L. Zhou, D. Wu, H. Peng, K. Yan, Y. Zhou, Z. Liu, *ACS Nano* **2011**, 5, 5957; i) A. Wei, J. Wang, Q. Long, X. Liu, X. Li, X. Dong, W. Huang, *Mater. Res. Bull.* **2011**, 46, 2131; j) H. Feng, R. Cheng, X. Zhao, X. Duan, J. Li, *Nat. Commun.* **2013**, 4, 1539; k) X. Dong, Q. Long, A. Wei, W. Zhang, L.-J. Li, P. Chen, W. Huang, *Carbon* **2012**, 50, 1517; l) H. Zhang, E. Bekyarova, J.-W. Huang, Z. Zhao, W. Bao, F. Wang, R. C. Haddon, C. N. Lau, *Nano Lett.* **2011**, 11, 4047.

[77] a) X. C. Dong, D. L. Fu, W. J. Fang, Y. M. Shi, P. Chen, L. J. Li, *Small* **2009**, 5, 1422; b) Q. H. Wang, M. C. Hersam, *Nat. Chem.* **2009**, 1, 206; c) Y. Zhu, Y. Hao, E. A. Adogla, J. Yan, D. Li, K. Xu, Q. Wang, J. Hone, Q. Lin, *Nanoscale* **2016**, 8, 5815; d) F. M. Koehler, N. A. Luechinger, D. Ziegler, E. K. Athanassiou, R. N. Grass, A. Rossi, C. Hierold, A. Stemmer, W. J. Stark, *Angew. Chem. Int. Ed.* **2009**, 48, 224; e) T. F. v. Dijkman, *Copper trispyrazolylborate complexes for ethene detection,* Doctoral Thesis Leiden University, **2016.** Retrieved from http://hdl.handle.net/1887/39518; f) C. Li, K. Komatsu, S. Bertrand, G. Clavé, S. Campidelli, A. Filoramo, S. Guéron, H. Bouchiat, *Phys. Rev. B* **2016**, 93, 045403; g) X. Wang, J.-B. Xu, W. Xie, J. Du, *J. Phys. Chem. C* **2011**, 115, 7596; h) Y. Y. Wang, P. J. Burke, *Nano Res.* **2014**, 7, 1650.

[78] a) N. Dontschuk, A. Stacey, A. Tadich, K. J. Rietwyk, A. Schenk, M. T. Edmonds, O. Shimoni, C. I. Pakes, S. Prawer, J. Cervenka, *Nat. Commun.* **2015**, 6, 6563; b) N. S. Green, M. L. Norton, *Anal. Chim. Acta* **2015**, 853, 127; c) N. Mohanty, V. Berry, *Nano Lett.* **2008**, 8, 4469; d) A. R. Gao, N. L. Zou, P. F. Dai, N. Lu, T. Li, Y. L. Wang, J. L. Zhao, H. J. Mao, *Nano Lett.* **2013**, 13, 4123; e) C.-T. Lin, P. T. K. Loan, T.-Y. Chen, K.-K. Liu, C.-H. Chen, K.-H. Wei, L.-J. Li, *Adv. Funct. Mater.* **2013**, 23, 2301.

[79] a) J. Wang, H. Zhu, Y. Xu, W. Yang, A. Liu, F. Shan, M. Cao, J. Liu, *Sens. Actuators. B* **2015**, 220, 1186; b) Q. Guo, H. Zhu, F. Liu, A. Y. Zhu, J. C. Reed, F. Yi, E.

Cubukcu, *ACS Photonics* **2014**, 1, 221; c) M. B. Lerner, F. Matsunaga, G. H. Han, S. J. Hong, J. Xi, A. Crook, J. M. Perez-Aguilar, Y. W. Park, J. G. Saven, R. Liu, A. T. C. Johnson, *Nano Lett.* **2014**, 14, 2709; d) S. Eissa, C. Tlili, L. L'Hocine, M. Zourob, *Biosens. Bioelectron.* **2012**, 38, 308.

[80] a) Y. Cui, S. N. Kim, S. E. Jones, L. L. Wissler, R. R. Naik, M. C. McAlpine, *Nano Lett.* **2010**, 10, 4559; b) J. Katoch, S. N. Kim, Z. F. Kuang, B. L. Farmer, R. R. Nalk, S. A. Tatulian, M. Ishigami, *Nano Lett.* **2012**, 12, 2342; c) L. Feng, L. Wu, J. Wang, J. Ren, D. Miyoshi, N. Sugimoto, X. Qu, *Adv. Mater.* **2012**, 24, 125; d) H. Zhang, Y. Wang, D. Zhao, D. Zeng, J. Xia, A. Aldalbahi, C. Wang, L. San, C. Fan, X. Zuo, X. Mi, *ACS Appl. Mater. Interfaces* **2015**, 7, 16152.

[81] a) S. Li, X. Zhong, H. Yang, Y. Hu, F. Zhang, Z. Niu, W. Hu, Z. Dong, J. Jin, R. Li, J. Ma, *Carbon* **2011**, 49, 4239; b) L.-M. Lu, H.-B. Li, F. Qu, X.-B. Zhang, G.-L. Shen, R.-Q. Yu, *Biosens. Bioelectron.* **2011**, 26, 3500; c) J. Luo, S. Jiang, H. Zhang, J. Jiang, X. Liu, *Anal. Chim. Acta* **2012**, 709, 47; d) B. C. Zhong, M. A. Uddin, A. Singh, R. Webb, G. Koley, *Appl. Phys. Lett.* **2016**, 108, 093102; e) F. Jimenez-Villacorta, E. Climent-Pascual, R. Ramirez-Jimenez, J. Sanchez-Marcos, C. Prieto, A. de Andrés, *Carbon* **2016**, 101, 305.

[82] K. S. Novoselov, D. Jiang, F. Schedin, T. J. Booth, V. V. Khotkevich, S. V. Morozov, A. K. Geim, *Proc. Natl. Acad. Sci. U. S. A.* **2005**, 102, 10451.

[83] a) V. Georgakilas, M. Otyepka, A. B. Bourlinos, V. Chandra, N. Kim, K. C. Kemp, P. Hobza, R. Zboril, K. S. Kim, *Chem. Rev.* **2012**, 112, 6156; b) F. Yan, M. Zhang, J. H. Li, *Adv. Healthcare Mater.* **2014**, 3, 313.

[84] K. Yang, L. Z. Feng, H. Hong, W. B. Cai, Z. Liu, *Nat. Protoc.* **2013**, 8, 2392.

[85] Z. X. Zhang, H. L. Huang, X. M. Yang, L. Zang, *J. Phys. Chem. Lett.* **2011**, 2, 2897.

[86] H. Tanveer, P. Puspamitra, A. Rajeev, *Nanotechnology* **2014**, 25, 325501.

[87] T. Hussain, P. Panigrahi, R. Ahuja, *Phys. Chem. Chem. Phys.* **2014**, 16, 8100.

[88] A. Y. S. Eng, Z. Sofer, P. Šimek, J. Kosina, M. Pumera, *Chem. Eur. J.* **2013**, 19, 15583.

[89] K. K. Tadi, S. Pal, T. N. Narayanan, *Sci. Rep.* **2016**, 6, 25221.

[90] X. Chia, A. Ambrosi, M. Otyepka, R. Zbořil, M. Pumera, *Chem. Eur. J.* **2014**, 20, 6665.

[91] V. Urbanová, K. Holá, A. B. Bourlinos, K. Čépe, A. Ambrosi, A. H. Loo, M. Pumera, F. Karlický, M. Otyepka, R. Zbořil, *Adv. Mater.* **2015**, 27, 2305.

[92] H. P. Boehm, A. Clauss, U. Hofmann, G. O. Fischer, *Zeitschrift Für Naturforschung B* **1962**, B 17, 150.

[93] D. A. Dikin, S. Stankovich, E. J. Zimney, R. D. Piner, G. H. B. Dommett, G. Evmenenko, S. T. Nguyen, R. S. Ruoff, *Nature* **2007**, 448, 457.

[94] a) S. Seo, M. Min, J. Lee, T. Lee, S. Y. Choi, H. Lee, *Angew. Chem. Int. Ed.* **2012**, 51, 108; b) S. Borini, R. White, D. Wei, M. Astley, S. Haque, E. Spigone, N. Harris, J. Kivioja, T. Ryhanen, *ACS Nano* **2013**, 7, 11166; c) X. H. Zhang, Y. Zhang, Q. L. Liao, Y. Song, S. W. Ma, *Small* **2013**, 9, 4045.

[95] A. Sinitskii, A. Dimiev, D. A. Corley, A. A. Fursina, D. V. Kosynkin, J. M. Tour, *ACS Nano* **2010**, 4, 1949.

[96] F. M. Koehler, N. A. Luechinger, D. Ziegler, E. K. Athanassiou, R. N. Grass, A. Rossi, C. Hierold, A. Stemmer, W. J. Stark, *Angew. Chem. Int. Ed.* **2009**, 48, 224.

[97] F. Karlicky, K. K. R. Datta, M. Otyepka, R. Zboril, *ACS Nano* **2013**, 7, 6434.

[98] a) E. Bekyarova, M. E. Itkis, P. Ramesh, C. Berger, M. Sprinkle, W. A. de Heer, R. C. Haddon, *J. Am. Chem. Soc.* **2009**, 131, 1336; b) D. E. Jiang, B. G. Sumpter, S. Dai, *J. Phys. Chem. B* **2006**, 110, 23628; c) Q. H. Wang, Z. Jin, K. K. Kim, A. J. Hilmer, G. L. C. Paulus, C. J. Shih, M. H. Ham, J. D. Sanchez-Yamagishi, K. Watanabe, T. Taniguchi, J. Kong, P. Jarillo-Herrero, M. S. Strano, *Nat. Chem.* **2012**, 4, 724; d) G. L. C. Paulus, Q. H. Wang, M. S. Strano, *Acc. Chem. Res.* **2013**, 46, 160; e) F. M. Koehler, W. J. Stark, *Acc. Chem. Res.* **2013**, 46, 2297; f) R. K. Shervedani, A. Amini, N. Sadeghi, *Biosens. Bioelectron.* **2016**, 77, 478; g) C. S. Rao Vusa, V. Manju, S. Berchmans, P. Arumugam, *RSC Adv.* **2016**, 6, 33409; h) M. Mooste, E. Kibena, J. Kozlova, M. Marandi, L. Matisen, A. Niilisk, V. Sammelselg, K. Tammeveski, *Electrochim. Acta* **2015**, 161, 195.

[99] S. D. Chakarova-Käck, E. Schröder, B. I. Lundqvist, D. C. Langreth, *Phys. Rev. Lett.* **2006**, 96, 146107.

[100] G. F. Schneider, Q. Xu, S. Hage, S. Luik, J. N. H. Spoor, S. Malladi, H. Zandbergen, C. Dekker, *Nat. Commun.* **2013**, 4, 2619.

[101] W. Sun, Y. Lu, Y. Wu, Y. Zhang, P. Wang, Y. Chen, G. Li, *Sens. Actuators. B* **2014**, 202, 160.

[102] a) F. K. Perkins, A. L. Friedman, E. Cobas, P. M. Campbell, G. G. Jernigan, B. T. Jonker, *Nano Lett.* **2013**, 13, 668; b) B. Cho, M. G. Hahm, M. Choi, J. Yoon, A. R. Kim, Y. J. Lee, S. G. Park, J. D. Kwon, C. S. Kim, M. Song, Y. Jeong, K. S. Nam, S. Lee, T. J. Yoo, C. G. Kang, B. H. Lee, H. C. Ko, P. M. Ajayan, D. H. Kim, *Sci. Rep.* **2015**, 5, 8052.

[103] a) L. Y. Feng, L. Wu, J. S. Wang, J. S. Ren, D. Miyoshi, N. Sugimoto, X. G. Qu, *Adv. Mater.* **2012**, 24, 125; b) J. P. Wang, B. J. Zou, J. Z. Rui, Q. X. Song, T. Kajiyama, H. Kambara, G. H. Zhou, *Microchim. Acta* **2015**, 182, 1095.

[104] a) X. S. Li, Y. W. Zhu, W. W. Cai, M. Borysiak, B. Y. Han, D. Chen, R. D. Piner, L. Colombo, R. S. Ruoff, *Nano Lett.* **2009**, 9, 4359; b) L. B. Gao, G. X. Ni, Y. P. Liu, B. Liu, A. H. C. Neto, K. P. Loh, *Nature* **2014**, 505, 190; c) Y. D. Su, H. L. Han, Q. Cai, Q. Wu, M. X. Xie, D. Y. Chen, B. S. Geng, Y. B. Zhang, F. Wang, Y. R. Shen, C. S. Tian, *Nano Lett.* **2015**, 15, 6501.

[105] a) W. H. Lin, T. H. Chen, J. K. Chang, J. I. Taur, Y. Y. Lo, W. L. Lee, C. S. Chang, W. B. Su, C. I. Wu, *ACS Nano* **2014**, 8, 1784; b) I. Pasternak, A. Krajewska, K. Grodecki, I. Jozwik-Biala, K. Sobczak, W. Strupinski, *AIP Adv.* **2014**, 4, 097133; c) G. Zhang, A. G. Güell, P. M. Kirkman, R. A. Lazenby, T. S. Miller, P. R. Unwin, *ACS Appl. Mater. Interfaces* **2016**, 8, 8008.